Insight into Biological Nitrile Reduction: A QM/MM Study of the Catalytic Mechanism of Nitrile Reductase

António J. M. Ribeiro[1], Lifeng Yang[2], Maria J. Ramos[1], Pedro A. Fernandes[1,*], Zhao-Xun Liang[2,*], and Hajime Hirao[3,*]

1. UCIBIO, REQUIMTE, Departamento de Química e Bioquímica, Faculdade de Ciências, Universidade do Porto, Rua do Campo Alegre s/n, 4169-007 Porto, Portugal
2. Division of Structural Biology & Biochemistry, School of Biological Sciences, Nanyang Technological University, Singapore
3. Division of Chemistry and Biological Chemistry, School of Physical and Mathematical Sciences, Nanyang Technological University, 21 Nanyang Link, Singapore 637371, Singapore

*E-mail: hirao@ntu.edu.sg, zxliang@ntu.edu.sg, pafernan@fc.up.pt

KEYWORDS: nitrile reductase; biocatalyst; transition-state, enzyme catalysis, covalent intermediate.

Abstract

The enzyme family of QueF nitrile reductases catalyzes the unprecedented four-electron reduction of nitrile to amine. QueF nitrile reductases can be found in the tRNA biosynthetic pathway of many bacteria and is considered to be a potential antimicrobial drug target. QueF enzymes also attract great attention as potential industrial biocatalysts for replacing the nitrile-reducing metal hydride catalysts used commonly in chemical and pharmaceutical industries. Because of their narrow substrate specificity, engineering of the QueF enzymes to generate variants with altered or broadened substrate specificity is crucial for producing practically useful biocatalysts. A better understanding of the catalytic mechanism of the QueF enzymes would expedite rational inhibitor design and enzyme engineering. In this work, we probed the catalytic mechanism of the *Vibrio cholerae* QueF nitrile reductase by state-of-the-art QM/MM calculation at the ONIOM(B3LYP/6-311+G(2d,2p):AMBER) level. The QM/MM computational results suggest that the nitrile-to-amine conversion proceeds through four major stages: a) formation of a C–S covalent bond between the substrate and the catalytic cysteine residue to form the thioimidate intermediate; b) hydride transfer from NADPH to the substrate to generate the thiohemiaminal intermediate; c) cleavage of the C–S covalent bond to generate the imine intermediate; d) second hydride transfer from NADPH to the imine intermediate to produce the final amine product. The free energy barrier for the rate-limiting step, *i.e.* the second hydride transfer, was found to be 20.8 kcal/mol. The calculated barrier height and catalytic residues identified as essential for nitrile reduction are in accordance with currently available experimental data. The computationally derived knowledge of the transition-state structures, intermediates and crucial protein conformational changes along the reaction path will be valuable for future design of enzyme inhibitors as well as the engineering of QueF nitrile reductases.

1. Introduction

QueF nitrile reductases were found from the biosynthetic pathway of queuosine (Q), a 7-deazaguanine modified nucleoside found exclusively at the wobble position of tRNAs. Although Q is crucial for the fidelity and efficiency of translation in both bacteria and eukarya, the Q biosynthetic pathways are only found in bacteria.[1,2] Within the Q-biosynthezing pathway, QueF catalyzes the NADPH-dependent reduction of the biosynthetic intermediate 7-cyano-7-deazaguanine ($preQ_0$) to 7-aminoethyl-7-deazaguanine ($preQ_1$) (Scheme 1).[3] Q-containing tRNAs are essential for the expression of the virulence genes of *Shigella flexneri*, without which the bacterium loses its pathogenicity.[4] Since *de novo* biosynthesis of Q occurs only in bacteria, the Q biosynthetic enzymes such as QueF nitrile reductase are potentially promising targets for the development of new antibacterial compounds. Meanwhile, compounds with a nitrile group are valuable synthetic precursors for obtaining amides, carboxylic acids and amines in chemical and pharmaceutical industries. Nitrile hydratases and nitrilases have already been successfully developed as enzyme biocatalysts for the transformation of nitriles into amides and carboxylic acids, respectively.[5–9] The nitrile-to-amine transformations are still catalyzed by using complex metal hydrides, which inevitably generate undesirable by-products and solvent waste.[10] The unexpected discovery of the QueF family of nitrile reductases raised the hope of developing environmentally sustainable biocatalysts for catalyzing the nitrile-to-amine transformation.[10–14]

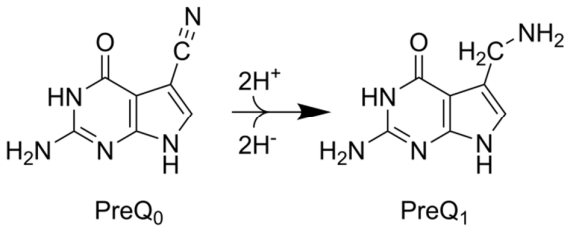

Scheme 1. The chemical reaction catalyzed by nitrile reductase through a four-electron reduction of the nitrile group of $preQ_0$.

Biochemical and structural characterization of QueF homologs from *Bacillus subtilis* (*B. subtilis*), *Vibrio cholerae* (*V. cholerae*), *Escherichia coli* (*E. Coli*), *Geobacillus kaustophilus* (*G. kaustophilus*) have yielded valuable insight into the mechanism of nitrile reduction.[15–20] Crystal

structures of the QueF homologs from *V. cholerae* and *B. subtilis* have been determined (PDB IDs: 3RJ4; 3BP1; 3UXJ; 3UXV; 4GHM; 4IQI; 4F8B)[15-17]. The crystal structures revealed that the QueF enzymes from *V. cholerae* and *B. subtilis* form a homodimer and homodecamer, respectively. The subunit of the dimeric *V. cholerae* QueF adopts a tunneling-fold or T-fold that is composed of four β-strands and two α-helices.[21] The binding mode of the substrate $preQ_0$ in the active site is determined from the crystal structure of the enzyme-substrate complex.[15–18] Although none of the current crystal structures contains the entire NADPH cofactor likely due to the mobility of the nicotinamide group, the position of the nicotinamide group can be inferred from the position of the diphosphate and ribose/adenine moieties. The crystal structures together indicate that the dimeric QueF only binds one NADPH molecule at a time, with the nicotinamide and adenine moieties of the NADPH cofactor situated in the two substrate-binding pockets. As a result, the nitrile reduction most likely occurs only in one monomer at a time. The crystal structures of *V. cholerae* QueF also reveal seven amino acid residues in the first coordination sphere of the substrate $preQ_0$ (Figure 1).[15–18] The side-chain groups of Glu94, Glu234, and Phe232, and the main-chain groups of Ser95 and Ile93 are directly involved in the binding of $PreQ_0$. The other three residues, Cys194, Asp201, and His233, are positioned next to the nitrile group of $PreQ_0$ and it has been suggested that they are the key catalytic residues.[15–17] Most importantly, Cys194 was proposed to function as a nucleophile to attack the nitrile group to form a thioimidate intermediate during catalysis. The involvement of the thioimidate intermediate was confirmed by the X-ray crystallographic observation of the covalent intermediate and the observation that Cys194 can be readily modified by iodoacetamide.[20] Mutagenic studies on the *E. coli* QueF showed that the only the two corresponding residues of Asp201 and Cys194 of *V. cholerae* QueF are essential for catalysis. [13]

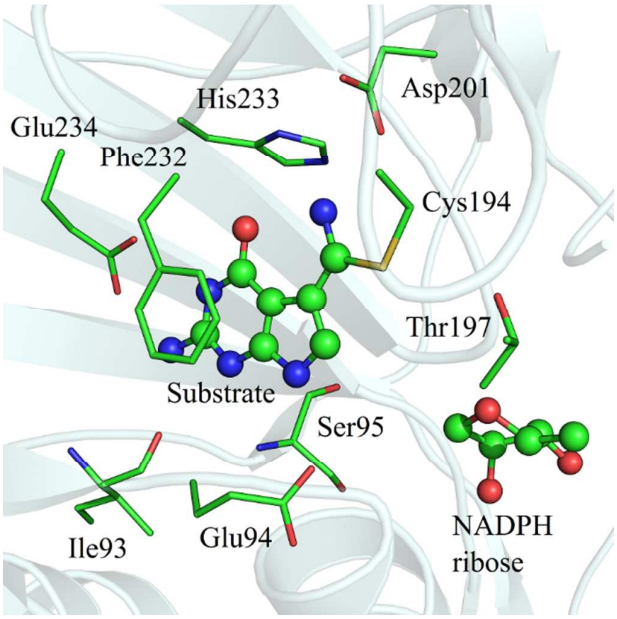

Figure 1. The active site of *V. cholerae* QueF nitrile reductase (PDB code 3UXJ). Catalytic and substrate-binding residues are shown in stick representation. The covalently attached $PreQ_0$ and the ribose group of NADPH are shown in ball-and-stick representation.

In this paper, we report the results from our QM/MM computational study of *V. cholerae* QueF and propose a reaction path for the unique nitrile reduction reaction catalyzed by QueF. We applied the ONIOM(B3LYP/6-311+g(2d,2p):AMBER) method to the structural model that contains two full subunits of *V. cholerae* QueF. This methodology has been widely used so far to probe the catalytic mechanisms of a diversity of enzymes.[22,23] We computationally examined four proposed steps that involve the formation of covalent intermediates and two NADPH-dependent reduction steps. The contribution of this work is threefold. Firstly, it provides insight into the highly unusual mechanism of NADPH-dependent nitrile reduction. Secondly, together with existing experimental data, our computational results elucidate the catalytic roles of the residues in the active site. This information shall be useful in future efforts in engineering QueF enzymes and designing new nitrile reductases as nitrile-reducing biocatalysts. Finally, the transition-state structures obtained from the calculations can be used for designing transition-state analogs that inhibit the growth of pathogenic bacteria and viruses.

2. Methods

We built a nitrile reductase model from a crystal structure (PDB code 3UXJ).[18 24] This structure contains two dimers of *V. cholerae* nitrile reductase. We chose only one dimer to proceed with the calculations. The dimer has two active centers, each containing the substrate, and shares a single $NADP^+$ molecule that occupies the active centers of both monomers. Only the active center that binds the nicotinamide group of NADPH is able to catalyze the reaction, and much attention has been focused on this center. The nicotinamide group is missing in the X-Ray structure, but its positioning can be determined reasonably from the arrangement of the rest of the NADPH molecule. The missing atoms were appended to the model using GaussView software.[25]

Two systems were defined within the enzyme according to the ONIOM scheme:[26–28] a model system to which quantum mechanics (QM) and molecular mechanics (MM) are applied and a real system (entire dimeric enzyme) to which MM is applied. The model system contained the entire 7-cyano-7-deazaguanine substrate, the nicotinamide and ribose groups of NADPH, and the side chains of Asp201, Cys194, His233, Glu234, and Thr197. The side chains of aspartate, glutamate, cysteine, histidine, and threonine were included in the model system as acetate, methanethiol, 5-methylimidazole, and ethanol, respectively. The truncated bonds were capped with hydrogen link (H-link) atoms. The exact size of the model system could differ in different steps depending on the presence of the NADPH molecule or the protonation states. The largest model contained 92 atoms, and the smallest contained 59 (both including the H-link atoms). The model system was described with the B3LYP[29,30] DFT functional and the 6-31G(d)[31] basis set in geometry optimization calculations. The point charges of the atoms outside the model system were included in the QM Hamiltonian according to the electrostatic embedding approach.

The real system was the entire dimer, although the first 26 amino acids of each subunit, which were not present in the X-ray structure and might not be very important for catalysis, were not included. The real system contained 8205 atoms in the models with NADPH, and 8160

atoms in the models without NADPH. The Amber parm96 force field parameters,[32] as implemented in Gaussian 09,[33] were used for amino acid residues. For the NADPH molecule, we used the parameters of Holmberg et al.[34–36] We derived parameters for 7-cyano-7-deazaguanine using antechamber software,[37] which is part of the Amber10 suite of programs.[38] Antechamber chooses bonds, angles, and van der Waals radii parameters from the GAFF force field,[39] based on the similarity to the structure being parameterized. Atomic point charges for the substrate were calculated using the HF/6-31G(d)[40] RESP (Restrained ElectroStatic Potential) method,[41] to maintain consistency with the rest of the Amber force field.

The potential energy surface was roughly explored first using appropriate internal coordinates of the substrate, co-factor, and catalytic residues. Subsequently, all minimum-energy states and transition states were optimized without any constraints. Frequency calculations were done to confirm the absence of imaginary frequencies in minimum-energy states and the existence of only one imaginary frequency in transition states. Values for zero-point-energy and entropy corrections were also computed. In order to improve the accuracy of the QM description, single-point energy calculations were performed at a higher level of theory, using B3LYP/6-311+G(2d,2p).[42–44] Atomic charges were calculated with the Charge Model 5 (CM5) extension of the Hirschfeld scheme,[45] as implemented in Gaussian. All calculations were carried out with Gaussian 09 software.[33] We used PyMOL,[46] VMD (Visual Molecular Dynamics),[47] and GaussView[25] as visualization tools.

3. Results and discussion

The overall mechanism of the nitrile reductase reaction was proposed to include four major stages: a) the formation of a C–S covalent bond between the substrate and the Cys194 residue; b) the transfer of a hydride ion from NADPH to the Cys-tethered intermediate; c) the cleavage of the C-S covalent bond and formation of an imine intermediate; and d) the transfer of a hydride ion from a second NADPH molecule to the imine intermediate.[10] With the exception of the first stage, which is supported by the experimental observation of the thioimidate

intermediate, the intermediates and transition states involved in the catalytic mechanism remain to be fully established. In addition, the precise role of His233, the identities of the residues that donate protons to the nitrile group, and the protonation states of residues and the substrate along the reaction pathway are unknown. Our computational results, which are obtained from extensive QM/MM calculations for the entire enzyme-NADPH-substrate complex, have yielded valuable mechanistic insights into the unique nitrile-reducing chemistry.

In the following sections, we present and discuss four individual reaction stages. In particular, we will analyze the activation and reaction free energies, relevant geometry parameters, and charge reorganization modes along the reaction path. Scheme 2 summarizes the overall reaction path bases on previous works. The intermediates and transition states in the pathway as well as other alternative pathways were subjected to close scrutiny in our QM/MM computational studies.

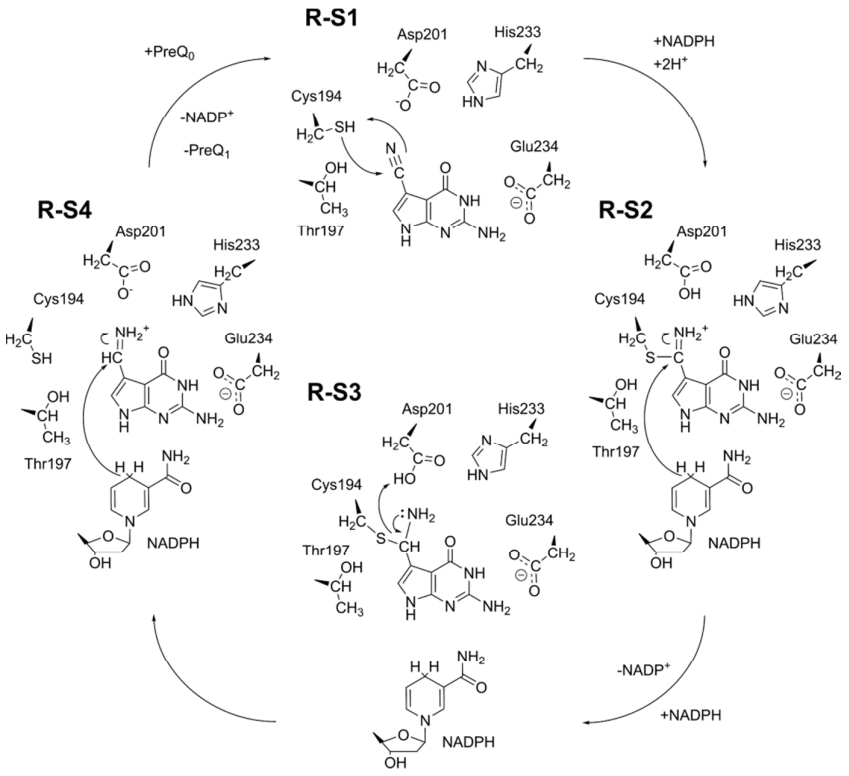

Scheme 2. Schematic representation of the four stages of the reaction catalyzed by nitrile reductase.

3.1. The catalytic mechanism

3.1.1. Stage 1: Formation of a covalent intermediate

Prior to the reduction of the nitrile group by the first hydride transfer from NADPH, a C-S bond is formed by the nucleophilic attack of the nitrile group of $preQ_0$ by Cys194. Formation of this covalent intermediate is supported by the observation of the thioimidate intermediate, and the covalent-bond formation is known to be independent of the presence of NADPH.[17,20] For this reason, we did not include NADPH in the model at this reaction stage. Scheme 3 shows the detailed reaction steps for this stage, with the optimized structures of all stationary states depicted in Figure 2. Tables I and II summarize the key interatomic distances and the charge distributions for these species, respectively.

In the reactant state of the first stage (R-S1), all the residues in the active site take on their normal protonation states: Asp201 and Glu234 are deprotonated and negatively charged, while His233, Cys194, Thr197, and the substrate are neutral. The stage of this reaction is initiated by a proton transfer from the thiol group of Cys194 to Asp201, which leads to the formation of an intermediate (INT1-S1). This proton transfer reaction involves a very early transition state; thus, the positions of the proton in R-S1 and in the transition state (TS-S1) are nearly the same, with the S–H distances being (1.44; 1.48; 2.08) Å and the H–O distances being (1.57; 1.46; 1.02) Å, where the three numbers in parentheses correspond to the distances for R-S1, TS-S1, and INT1-S1, respectively. The hydroxyl group of Thr197 is likel to play an important role in stabilizing the negatively charged thiolate form of Cys194. As the proton transfer progresses, the distance between hydroxyl and the sulfur decreases (r(H–S) = (2.70; 2.61; 2.24) Å). On the other hand, the interaction between one of the carboxylic oxygen atoms of Asp201 and the proton on the ε-nitrogen of His233 is weakened slightly ((r(O–H) = (1.97; 2.00; 2.28) Å), likely because Asp201 is no longer negatively charged after the proton transfer. The free energy barrier for this proton transfer process is very small (0.8 kcal/mol), with an overall negative free energy of -3.5 kcal/mol. Hence, the state with ionized Cys194 resulted from the proton transfer process is more stable than the state with the ionized Asp201 and neutral Cys194.

In the proton-transfer step, Asp201 gains half of a positive charge (charge(Q) = (-0.69; -0.58; -0.20)), which comes mostly from Cys194 (Q = (-0.20; -0.31; -0.62)). Thr197 and His233 also contribute to this new charge distribution by accepting a small amount of negative charge from the cysteine, and a small amount of positive charge from Asp201. As can be seen in Figure 2, the negative charge that Cys194 gains is localized primarily on the sulfur atom, and the negative charge of Thr197 is concentrated mostly on the hydroxyl proton. In contrast, the calculation revealed that the newly developed positive charge on Asp201 and His233 is delocalized over their side chains.

The geometry of INT1-S1 is not optimized for the nucleophilic attack of the thiolate on the nitrile carbon atom. In order for the intermediate to proceed to the next reaction, the active site needs to undergo significant conformational change to reach the INT2-S1 state. The conformational change is thermodynamically more factorable, with INT2-S1 9.3 kcal/mol more stable than INT1-S1. In INT2-S1, Cys194 and Asp201 are closer to the –CN group and in better positions for the next step of the reaction. The carboxylic oxygen atoms of Asp201 is located very far from the nitrogen atom of the nitrile (r(H–N) = 4.93 Å) in INT1-S1, but now the carboxylic oxygen atoms are positioned next to the nitrogen atom in INT2-S1 (r(N–H) = 1.67 Å) within hydrogen bond distance. This conformational change to INT2-S1 alters the charge distribution in a manner that is more favorable for the subsequent nucleophilic attack: Cys194 and Thr197 become more negative and likely more nucleophilic, whereas the carbon center of the nitrile group becomes more positive.

The last step of this reaction stage involves the formation of a transition state (TS2-S1) for the nucleophilic addition reaction and a covalent thioimidate intermediate (P-S1). In the thioimidate intermediate, the substrate $preQ_0$ becomes covalently tethered to the enzyme via Cys194. The C–S distances are (3.80; 2.31; 1.88) Å for INT2-S1, TS2-S1, and P-S1, respectively. Additionally, our calculation suggest that Asp201 is the likely the general-acid catalyst, with the carboxylic proton of Asp201 is transferred to the nitrogen atom of the nitrile group (r(N–H) = (1.67; 1.12; 1.03) Å). After the formation of the thioimidate intermediate, the N-C triple bond is converted to a double bond (r(N–C) = (1.16; 1.19; 1.25) Å). The interaction

between the two conserved His233 and Asp201 residues is restored to the one in the initial conformation, with Asp201 losing its proton to become negatively charged again.

During the C-S bond formation, Asp201 and Cys194 are seen to undergo the largest changes in charge distribution within the active center. Asp201 becomes negatively charged as it donates its proton to the substrate, and Cys194 loses about the same amount of negative charge when it becomes covalently linked to the substrate. Close inspection of the atomic charges shows that the sulfur atom of Cys194 exhibits significant change in electron density. The negative charge is lost from Cys194 predominantly through the sulfur atom. The loss of positive charge from Asp201 should occur through the leaving carboxylic proton, since the charge of all its atoms (including the proton) barely changes. As for the substrate, the nitrile group is responsible for accommodating most of the electronic density that is transferred to the substrate.

With respect to INT2-S1, the free energy barrier for this step is 19 kcal/mol and the reaction free energy is 13.7 kcal/mol; whereas in relation to the initial reactants, the barrier and reaction energy are 6.2 and 0.9 kcal/mol, respectively.

Table I. Relevant interatomic distances (in Å) for the first stage of the nitrile reductase mechanism: the formation of the covalent intermediate

	R-S1	TS1-S1	INT1-S1	INT2-S1	TS2-S1	P-S1
Nitrile C – Nitrile N	1.16	1.16	1.16	1.16	1.19	1.25
Nitrile C – Cys194 S	3.88	3.92	3.98	3.80	2.31	1.88
Nitrile N – Asp201 H	4.72	4.74	4.93	1.67	1.12	1.03
Thr197 H – Cys194 S	2.70	2.61	2.24	2.17	2.17	2.27
Asp201 H – Asp201 O	1.57	1.46	1.02	1.01	1.42	1.84
Cys194 S – Cys194 H	1.44	1.48	2.08	4.96	3.71	3.01
His233 H – Asp201 O	1.97	2.00	2.28	2.27	2.02	2.07

Table II. Absolute atomic charges grouped by residues for the first stage of the nitrile reductase mechanism: the formation of the covalent intermediate. Only QM residues whose charge changes significantly are included

	R-S1	TS1-S1	INT1-S1	INT2-S1	TS2-S1	P-S1
Substrate	-0.26	-0.26	-0.26	-0.12	-0.15	-0.21
Asp201	-0.69	-0.58	-0.20	-0.11	-0.50	-0.77
Cys194	-0.20	-0.31	-0.62	-0.74	-0.34	-0.06
His233	-0.14	-0.13	-0.09	-0.09	-0.13	-0.13
Thr197	-0.01	-0.02	-0.13	-0.23	-0.18	-0.12

The charge of the thiol proton was divided into halves and distributed to Cys194 and Asp201 in the first transition state; and between Asp201 and the substrate in the second transition state.

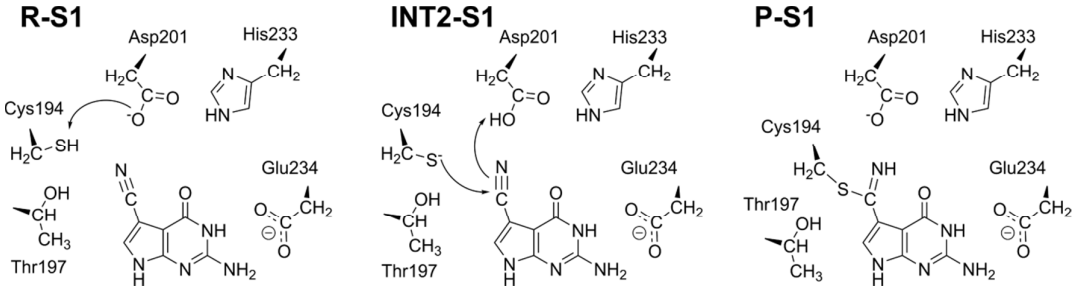

Scheme 3. Schematic representation of the first stage of the nitrile reductase reaction mechanism: the formation of the covalent intermediate between the substrate and Cys94.

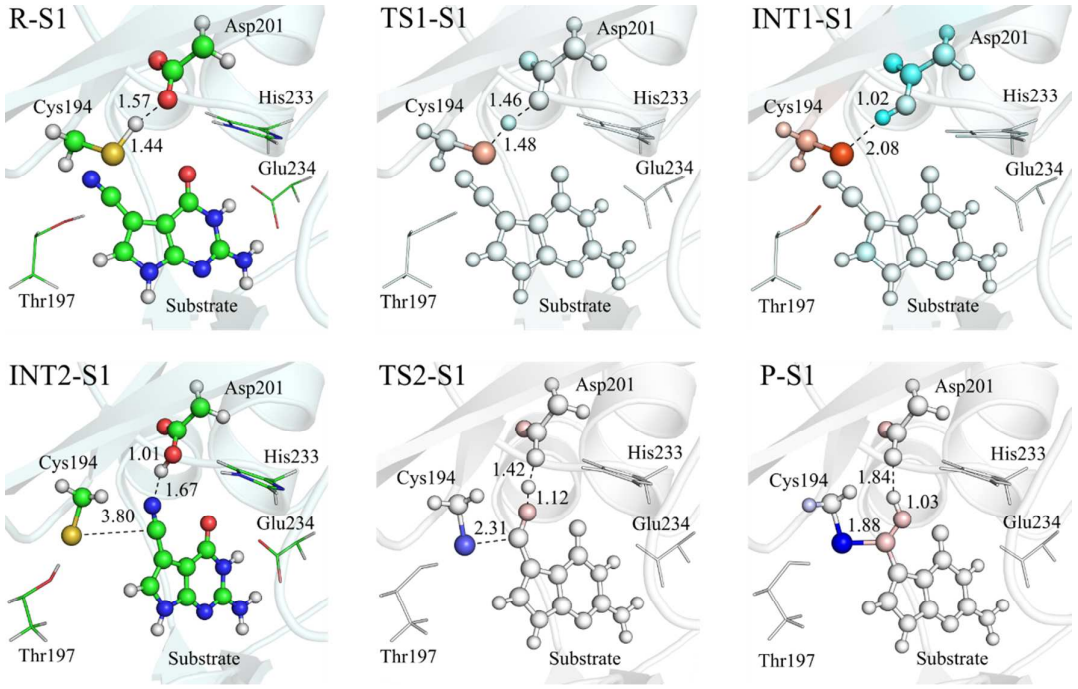

Figure 2. Optimized structures for the first stage of the nitrile reductase reaction mechanism. Only the QM-layer atoms are explicitly shown in the pictures. The coloring of TS1-S1, INT1-S1, TS2-S1, and P-S1 represents the difference of point atomic charges between that state and the previous minima. The red color means that the atom became more negatively charged, and the blue color indicates that the atom became more positively charged.

3.1.2. Stage 2: First hydride transfer

The second stage of the catalytic mechanism involves the reduction of the thioimidate intermediate by a hydride from the co-substrate NADPH. To reduce the thioimidate intermediate (P-S1) generated from the first stage, an NADPH molecule and two protons must

be supplied to the reaction center (Scheme 2). These protons originate most probably from the surrounding aqueous environment, since there is no suitable residue in the vicinity that could possibly act as proton donors. The overall charge of the active center decreases by two after the addition of the NADPH (-4 charge) and the two protons (+1 charge each).

We examined a few possibilities concerning the protonation states of the nitrile group and Asp201. In particular, a mechanism that seems plausible involves the donation of a proton from Asp201 to the neutral nitrile group during hydride transfer. The energetics of this mechanism, however, does not agree with the experimental k_{cat} or typical catalytic barriers. More information about this alternative mechanism is given in the Supporting Information.

The alternative mechanism, which involves the protonation of the thioimidate intermediate, seems to be more reasonable energetically. For the reactant state of this more reasonable mechanism (R-S2), the carboxyl group of Asp201 and the nitrogen atom of the thioimidate are first protonated (see Scheme 4). The nicotinamide group of NADPH now occupies the previously empty space of the active center, and is positioned side by side with the substrate (see Figure 3). The hydride transfer reaction occurs in a single step, and the distances between the transferring hydride and the hydride-accepting carbon atom (r(C–H)) are 3.07, 1.55 and 1.09 Å for R-S2, TS-S2, and P-S2 respectively. Table III lists other relevant geometric parameters for this reaction stage. The distance between the hydride and the nicotinamide carbon increases accordingly ((1.11; 1.28; 2.69) Å). These values suggest that this stage involves an early transition state (TS1-S2), at which point the hydride is closer to the NADPH molecule (1.28 Å) than to the $C{=}NH_2$ group (1.55 Å). At TS-S2, the angle subtended by these three atoms is large (171.3º). As the C=N double bond becomes C-N bond and the C–N distance increases accordingly (r(C–N) = (1.33; 1.41; 1.47)), we observe some small changes that accompany the hydride movement, which are likely required to facilitate the hydride-transfer process. For example, the bond between the sulfur atom of Cys194 and the carbon atom of $C{=}NH_2^+$ group is also elongated (r(S–C) = (1.76; 1.79; 1.86) Å) to accommodate the additional electronic density. The hydrogen bond between the nitrogen atom of $C{=}NH_2^+$ and the carboxylic hydrogen of Asp201 is shortened and most likely strengthen (r(N–H) = (2.15; 1.70; 1.57) Å). The other

hydrogen bond between the ε nitrogen atom of His233 and the amine group of nicotinamide also shortens (r(N–H) = (2.79; 2.03; 2.21) Å), suggesting that the slightly basic histidine residue plays a role in stabilizing the formation of the positive nicotinamide group. The activation free energy for this reaction step was found to be 19.1 kcal/mol, with a negative reaction free energy of -15.9 kcal/mol.

An analysis of the charge distribution along the reaction path provides some interesting clues about the origin of transition state stabilization. Differences in the atomic partial charges are shown in Figure 3. Table IV shows the absolute atomic charges grouped by residues. Along the reaction path, the NADPH molecule loses one negative charge, which is compatible with the transfer of a hydride (Q = (-0.02, 0.38, 0.87)). The initial and final negative charge of NADPH is not delocalized over other residues, indicating that both NADPH and $NADP^+$ are relatively stable. The additional positive charge of $NADP^+$ is uniformly distributed over the nicotinamide group, but some localization on the aromatic ring is observed. By contrast, the thioimidate intermediate has only a partial positive charge of 0.55, in the R-S2 state. The rest of the positive charge is delocalized onto Cys194, which is covalently bonded to the $C{=}NH_2$ group, and onto Glu234, which is now less negative. The differences in charge distributions among R-S2, TS-S2, and P-S2 allow us to identify which residues contribute significantly to the catalysis by accepting some of the negative charge of the hydride. In this case, Asp201 and Cys194 are important, becoming *circa* 0.2 more negative along the reaction path. His233, Thr197, and Glu234 maintain roughly the same charge. Within the thioimidate intermediate, the C and N atoms of the $C{=}NH_2$ group accept more negative charge than the other atoms. The sulfur atom and the carboxylic oxygen atoms accept the negative charge to the greatest extent in Cys194 and Asp201, respectively.

Table III. Relevant interatomic distances (in Å) and angles (in degrees) for the second stage of the nitrile reductase reaction: the first hydride transfer

	R-S2	TS-S2	P-S2
Nitrile C – Nitrile N	1.33	1.41	1.47
Nitrile C – Cys194 S	1.76	1.79	1.86
Nitrile C – H^-	3.07	1.55	1.09
NADPH C – H^-	1.11	1.28	2.69
Nitrile N – Asp201 H	2.15	1.70	1.58
His233 N – NADPH H	2.79	2.04	2.22
Nitrile C – H^- – NADPH C	136	171	156

Table IV. Absolute atomic charges grouped by residues for the second stage of the nitrile reductase mechanism: the first hydride transfer. Only QM residues whose charge changes significantly are included

	R-S2	TS-S2	P-S2
NADPH	-0.02	0.38 [a]	0.87
Substrate	0.55	0.30 [a]	0.04
Asp201	0.02	-0.10	-0.17
Cys194	0.10	0.06	-0.08

[a] We divided the charge of the hydride ion evenly between the NADPH and the substrate in the transition state.

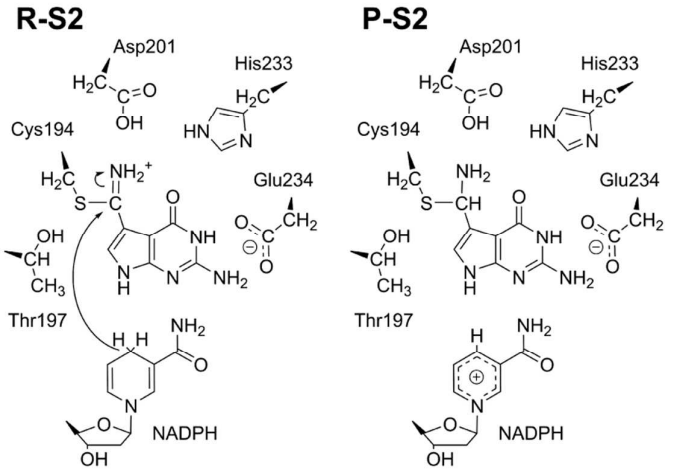

Scheme 4. Schematic representation of the second stage of the nitrile reductase mechanism: the hydride transfer from the first NADPH molecule to the nitrile group.

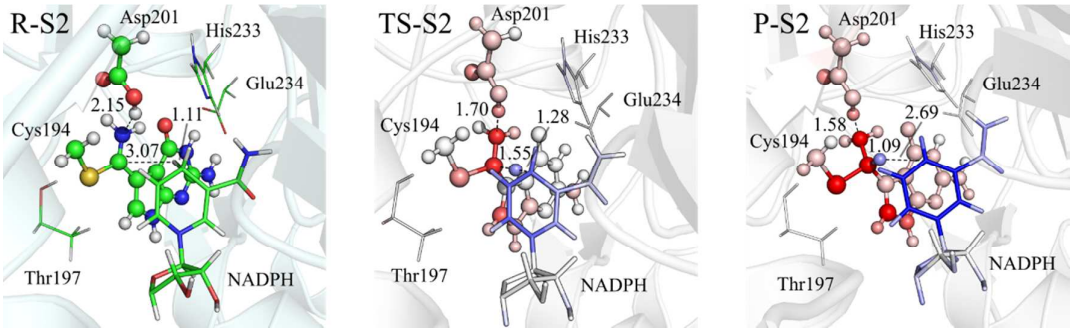

Figure 3. Optimized structures for the second stage of the nitrile reductase mechanism. Only the QM-layer atoms are explicitly shown in the pictures. The coloring of TS1-S2 and P-S2 represents the difference of point atomic charges between that state and the reactants. The red color means that the atom became more negatively charged, and the blue color indicates that the atom became more positively charged.

3.1.3. Stage 3: Cleavage of the C–S bond

Before the second hydride transfer, the $NADP^+$ ion must be replaced with another NADPH molecule. It is also proposed that and the covalent C–S bond must be broken to generate an imine intermediate. Although theoretically it is possible to generate the final amine product directly from the thiohemiaminal intermediate by a S_N2 reaction mechanism with the hydride as nucleophile, our modeling suggested that such mechanism is not reasonable because of the severe steric hindrance caused by the Cys194 residue. If the C–S bond is not broken first, Cys194 will sterically prohibit the nicotinamide moiety from approaching the covalent-attached intermediate. We modelled this C-S bond-breaking process with NADPH bound in the active center. The presence of NADPH could be important for two reasons. First, because the imine intermediate is prone to hydrolysis in the presence of a water molecule, the presence of NADPH could be crucial for protecting the imine from H_2O and safeguarding the turnover of imine to amine. Second, NADPH may play a role by maintaining or pre-organizing the active center in an optimal conformation and charge distribution. Scheme 5 depicts the individual steps from this stage, with Figure 4 showing the optimized reactant, transition state and product structures for each step. The main interatomic distances and the charge distributions are included in Tables V and VI respectively.

In the reactant state of this reaction (R-S3), the side chain of Asp201 is protonated while all other residues in the active center have their default protonation states. Apart from the

change from $NADP^+$ to NADPH, there is no other significant change in the active center, compared with P-S2 in the first hydride-transfer reaction. During the first step of this stage (from R-S3 via TS1-S3 to INT-S3), the bond between the sulfur atom of Cys194 and the carbon atom of the original nitrile group is broken (r(C–S) = (1.97; 2.39; 3.19) Å). It is the side chain of Asp201 that contributes most to the stabilization of the transition state by maintaining and gradually strengthening the hydrogen bond with the sulfur atom during the step (r(S–H) = (2.27; 2.20; 2.09) Å). The hydroxyl group of Thr197 can also form a hydrogen bond with the sulfur atom, but only in the final intermediate state (r(S–H) = (4.64; 4.45; 2.49) Å). The change of bond order from C-N to C=N is apparent. Not only has the bond length decreased (r(C–N) = (1.42; 1.35; 1.30) Å), but the nitrogen atom has also changed from sp^3 to a planar sp^2 configuration (Figure 4). The activation free energy for this step is 4.9 kcal/mol and this step is slightly favorable, with a reaction free energy of -2.3 kcal/mol.

Calculated charge distributions (Table VI) clearly show that the charge polarization increases as the distance between the sulfur and carbon atoms becomes larger. In the thiohemiaminal intermediate, the substrate carries half of a positive charge, while Cys194 has half of a negative charge. All other residues in the active center remain neutral. In terms of the atomic charges (Figure 4), the sulfur harbors most of the new negative charge in Cys194, while the new positive charge of the reactant is mostly localized on the $N_{C\text{-}NH2}$ atom, followed by the $C_{C\text{-}NH2}$ atom, and then the 7-deazapurine moiety. Asp201 is not completely inert, as the noticeable change in its overall charge suggests. A slight polarization between its carboxylic proton and the deprotonated carboxylic oxygen atom was also observed.

In the second step of this stage, the negatively charged Cys194 accepts a proton from Asp201. The transition state (TS2-S3) is a very early one, at which the Asp201 proton has moved only slightly from the carboxylic oxygen atom, as can be seen from the r(O–H) distances of (1.03; 1.16; 3.96) Å for INT-S3, TS2-S3, and P-S3, respectively. The distance between the proton and the sulfur atom decreases accordingly (r(S–H) = (2.09; 1.76; 1.35) Å). The other two interactions, *i.e.* the interactions between Thr197 and Cys194 and between Asp201 and the nitrile, change significantly along this path, especially in a late stage: the hydroxyl group of

Thr197 moves away from the sulfur atom, now that the sulfur is no longer negatively charged (r(S–H) = (2.49; 2.57; 3.78) Å); and the now negatively charged Asp201 carboxylic group becomes tightly bound to the positive nitrile group of the substrate (r(O–H) = (2.19; 1.94; 1.62) Å). The energy of TS2-S3 is 2.9 kcal/mol relative to INT1-S3 and -0.6 kcal/mol relative to R-S3. This step has a large reaction energy of -24.3 kcal/mol relatively to INT1-S3 and -22.9 kcal/mol relatively to P-S3. This substantial reaction energy may not be accounted for by the proton transfer alone, but it may be largely due to the formation of a favorable ionic bond between Asp201 and the -NH_2 group.

The charge variations at TS2-S3 are rather small (see TS2-S3 in Table VI and Figure 4) and are solely concentrated on the sulfur atom of Cys194 and the carboxylic proton of Asp201. However, in the product state, the charge delocalization is more extensive. Asp201 contains more than half of a negative charge, dispersed over its side chain, and Cys194 is now neutral. Thr197, another residue located in the active site, also accepts some charge from the sulfur atom.

Table V. Relevant interatomic distances (in Å) for the third stage of the nitrile reductase reaction: the breaking of the covalent intermediate.

	R-S3	TS1-S3	INT1-S3	TS2-S3	P-S3
Nitrile C – Nitrile N	1.42	1.35	1.30	1.30	1.30
Nitrile C – Cys194 S	1.97	2.39	3.19	3.24	3.36
Asp201 O – Nitrile H	3.67	3.43	2.19	1.94	1.62
Thr197 H – Cys194 S	4.64	4.45	2.49	2.57	3.78
Asp201 H – Asp201 O	1.00	1.01	1.03	1.16	3.96
Asp201 H – Cys194 S	2.27	2.20	2.09	1.76	1.35
His233 H – Asp201 O	2.06	1.98	2.12	2.07	1.99

Table VI. Absolute atomic charges grouped by residues for the third stage of the nitrile reductase mechanism: the breaking of the covalent intermediate. Only QM residues whose charge changes significantly are included.

	R-S3	TS1-S3	INT1-S3	TS2-S3	P-S3
Substrate	0.04	0.26	0.58	0.58	0.54
Asp201	-0.10	-0.12	-0.14	-0.35[a]	-0.68
Cys194	-0.09	-0.33	-0.58	-0.37[a]	-0.05
His233	-0.11	-0.11	-0.09	-0.10	-0.14
Thr197	0.04	0.04	-0.06	-0.03	0.04

[a] We divided the charge of the Asp201 proton into halves and distributed the split charges to Cys194 and Asp201 at TS2-S3.

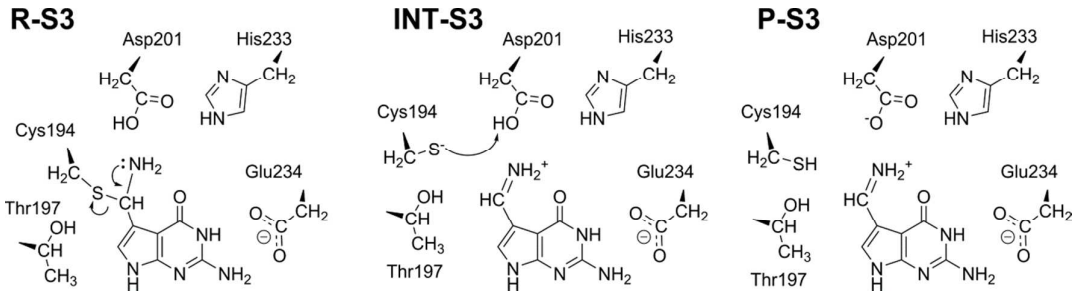

Scheme 5. Schematic representation of the third stage of the nitrile reductase reaction mechanism: the breaking of the covalent intermediate between the substrate and Cys94. NADPH is present in the QM layer of this QM/MM model but is not shown here for simplicity.

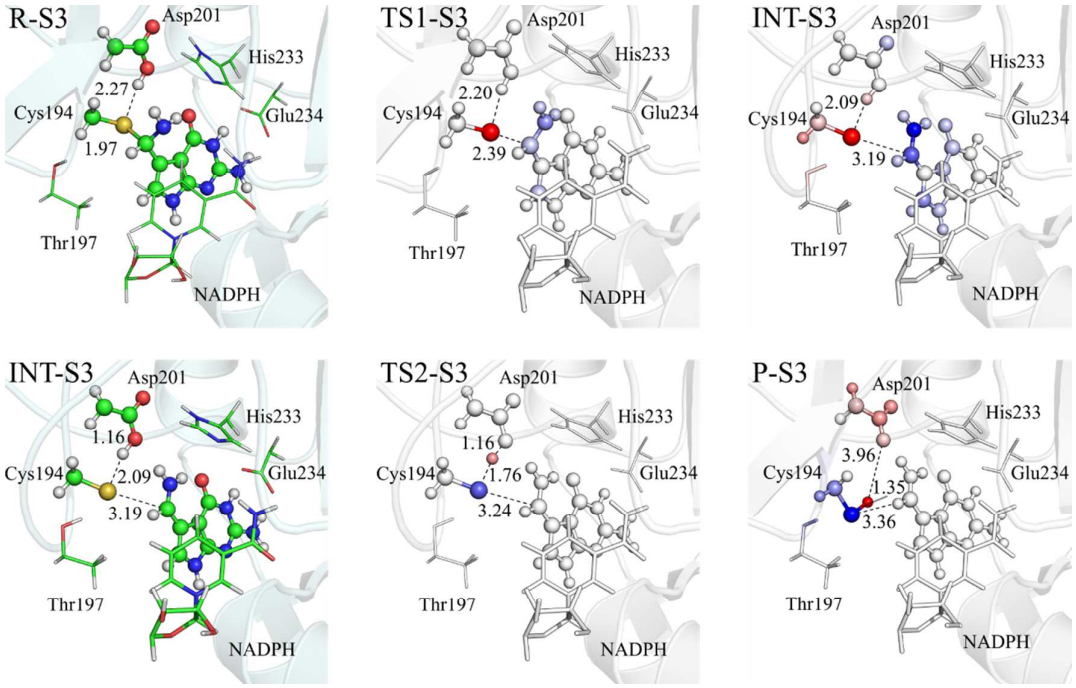

Figure 4. Optimized structures for the third stage of the nitrile reductase reaction mechanism. Only the QM-layer atoms are explicitly shown in the pictures. The coloring of TS1-S3, INT-S3, TS2-S3, and P-S3 represents the difference of point atomic charges between that state and the previous minima. The red color means that the atom became more negatively charged, and the blue color indicates that the atom became more positively charged. The structure of INT is shown twice, but in different representations.

3.1.4. Stage 4: Second hydride transfer

The last step of the reaction involves the transfer of a second hydride to the imine intermediate from NADPH. The reactant state for this stage is essentially the same as P–S3 from the previous stage. The negatively charged Asp201 interacts strongly with the positively charged imine group of the substrate, and all the other residues are in their normal protonation states. In our calculations, although the structures of R-S4 and P-S3 are not exactly the same because they are located in different energy minima, the main geometrical parameters in the active center are very similar. Scheme 6 illustrates the reaction steps of this stage, and Figure 5 shows the optimized structures of all stationary states. Tables VII and VIII summarize the key interatomic distances and the charge distributions, respectively.

The hydride transfer from the nicotinamide group of NADPH to the imine group of the intermediate occurs in a single step. The r(C(nitrile)–H) values are (2.50; 1.28; 1.11) Å for R-S4, TS-S4, and P-S4, respectively, and the r(C(NADPH)–H) values are (1.10; 1.50; 2.72) Å. Thus, at the transition state (TS-S4), the hydride is closer to the carbon atom of imine than to the nicotinamide carbon of NADPH. This late transition state is in contrast to the early transition state of the first hydride transfer, which explains why the barrier is lower for the second hydride transfer. The arrangement of these three atoms is also less linear than in the first hydride transfer reaction: (angle = (141; 154; 108) (^{o}), compared with (136; 171; 156) (^{o}) for the first reduction. The C=N double bond of the intermediate is reduced to yield the N-H single bond during the reaction, which is evident from the increase in bond length (r(C–N) = (1.30; 1.38; 1.47) Å and the change of hybridization from planar sp^2 to tetrahedral sp^3 for the nitrogen atom. The interaction between Asp201 and the nitrile nitrogen is significantly reduced as the reaction progresses (r(H–N) = (1.70; 1.91; 2.10) Å. On the other side of the carboxylic group of Asp201, the interaction between the oxygen and the NH moiety of His233 becomes stronger (r(O–H) = (2.97; 2.12; 2.13) Å). Concomitantly, the interaction between the δ-nitrogen of His233 and the amide group of NADPH is also strengthened (r(N–H) = (2.97; 2.12; 2.13) Å). Hence, it seems that Asp201 also helps stabilize the newly formed positive charge on NADPH,

though it is not as efficiently as the imine group does. The activation free energy of this step is 20.8 kcal/mol, with a reaction free energy is 10.8 kcal/mol.

The change in charge distribution is consistent with the way the geometrical parameters change. The NADPH molecule becomes increasingly positive with the progress of the reaction (Q = (-0.01; 0.46; 0.83)), while the substrate receives most of the negative charge (Q = (0.53; 0.09; -0.22)). The overall charge of the rest of the residues hardly changes. In Figure 5, we can see that the positive charge of $NADP^+$ is well delocalized over the nicotinamide ring, while the charge on the substrate is mostly concentrated on the imine group. Nevertheless, other parts of NADPH and the substrate also undergo slight variations in the charge. Some of the negative charge of the substrate goes to the five-membered ring of the 7-deazapurine, and the amide and ribose groups of the NAPDH also receive some amounts of positive charge. The interaction between the amide group of NADPH and His233 seems to be significantly strengthened as the reaction progresses. The negatively charged Asp201 is likely to stabilize the accumulating charge in the amide group indirectly through this bridging histidine residue.

Table VII. Relevant interatomic distances (in Å) and angles (in degrees) for the fourth stage of nitrile reduction, i.e. the second hydride transfer.

	R-S4	TS-S4	P-S4
Nitrile C – Nitrile N	1.30	1.38	1.47
Nitrile C – Cys194 S	3.33	3.46	3.39
Nitrile C – Hydride	2.50	1.28	1.11
NADPH C – hydride	1.10	1.50	2.72
Nitrile H – Asp201 O	1.70	1.91	2.10
His233 N – NADPH amide H	2.97	2.12	2.13
His233 H - Asp201 O	2.52	2.37	2.16
Nitrile C – Hydride – NADPH C	141	154	108

Table VIII. Absolute atomic charges grouped by residues for the fourth stage of the nitrile reductase mechanism: the second hydride transfer. Only QM residues whose charge changes significantly are included.

	R-S4	TS-S4	P-S4
NADPH	-0.01	0.46 [a]	0.83
Substrate	0.53	0.09 [a]	-0.22
Asp201	-0.75	-0.79	-0.80
Cys194	-0.06	-0.06	-0.08
His233	-0.07	-0.03	-0.04

[a] We divided the charge of the hydride ion into halves and distributed them to the NADPH and the substrate at TS-S4.

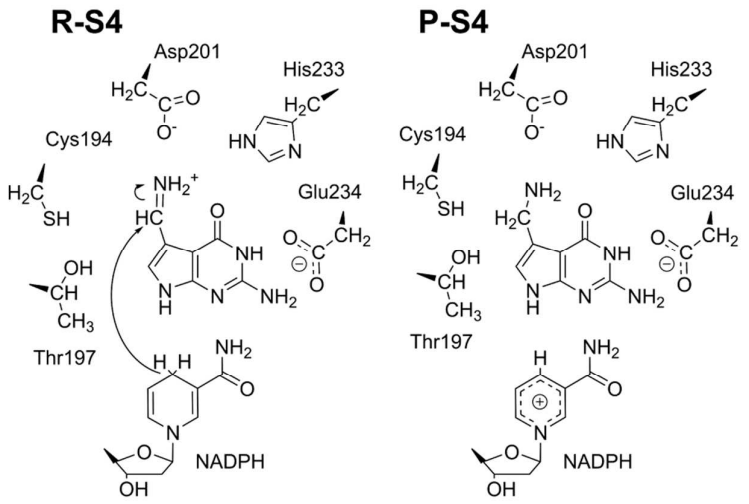

Scheme 6. The fourth stage of the nitrile reductase mechanism: the hydride transfer from the second NADPH molecule to the nitrile group.

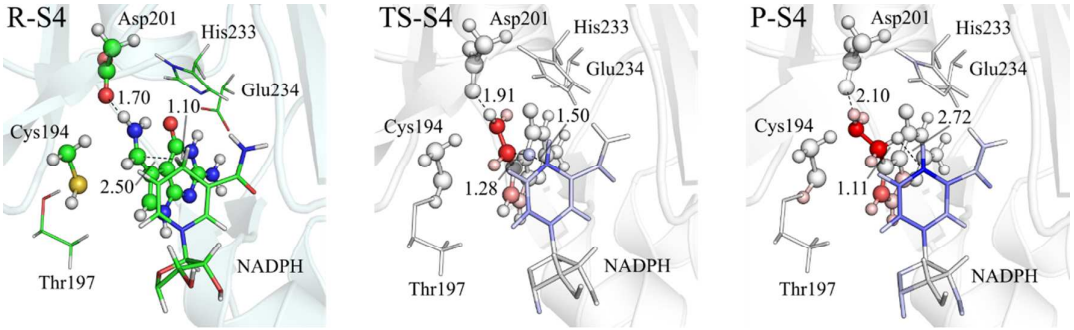

Figure 5. Optimized structures for the fourth stage of the nitrile reductase mechanism. Only the QM-layer atoms are explicitly shown in the pictures. The coloring of TS1-S4 and P-S4 represents the difference of point atomic charges between that state and the reactants. The red color means that the atom became more negatively charged, and the blue color indicates that the atom became more positively charged.

And finally, the free energy profiles for the four reaction stages obtained from our calculation are summarized in the Figure 6. The barriers for stages 1, 2, 3 and 4 are 19.0, 19.1, 4.9 and 20.8 kcal/mol respectively. The second hydride transfer occurred in stage 4 constitutes the rate-limiting step of the overall reaction. Stage 3 was found to be the process associated with the lowest kinetic barriers.

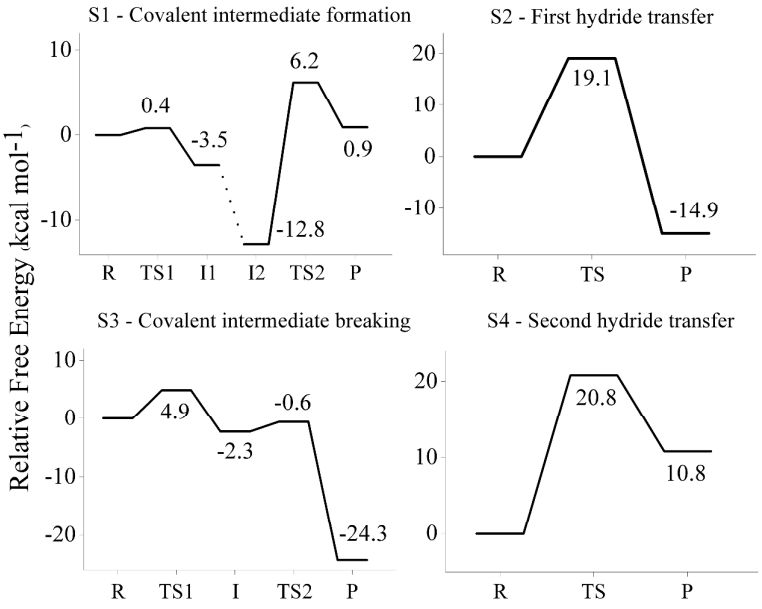

Figure 6. Free energy profiles for the 4 stages of the nitrile reductase reaction.

3.2. Comparison with experimental kinetic data

The above calculations identified the rate-limiting step of the catalytic reaction of nitrile reductase as the second hydride transfer via TS-S4, which has an energy barrier of 20.8 kcal/mol. The barrier for the first hydride transfer via TS-S2 is almost as high, with the value being 19.1 kcal/mol. These values agree well with the available data on the experimental turnover of nitrile reductase enzymes. Although there is no published value of k_{cat} for the *V. cholerae* enzyme, to the best of our knowledge, we can use the k_{cat} values for the enzymes of *B. subtilis,*[20,21] *E. coli,*[13,14] *and G. kaustophilus.*[12] The enzyme turnovers of these organisms are 0.011 s^{-1} (at 30 ºC), 0.12 s^{-1} (at 30 ºC), and 0.065 s^{-1} (at 55 ºC), respectively. These values are converted to free energy barriers of 20.5, 19.0, and 20.7 kcal/mol, according to transition state theory. The similarity of the active centers of the four enzymes indicates that the turnover number for *V. cholerae* is not very different.

The rate-limiting step of the formation of the covalent intermediate is the nucleophilic attack of the negative sulfur atom of Cys194 on the substrate (TS2-S1), and the free energy barrier for this step is 19.0 kcal/mol. Since the formation of the covalent intermediate is not

dependent on NADPH, it is possible to stop the reaction at P-S1 by not adding the NADPH to the reaction mixture. The trap of the thioimidate intermediate is demonstrated in an experimental study,[17] and the rate of the thioimidate formation was estimated to be in the order of 2 s^{-1}, which corresponds to a barrier of 17.8 kcal/mol. This value agrees very well with our calculations.

In stage 4, P-S4 is less stable than the previous intermediate. Since the reaction is expected to be spontaneous, there must be additional reaction steps or contributions to the energy that lead to an overall exergonic reaction. The contribution could come from the entropic energy gain resulting from the release of the $preQ_1$ and $NADP^+$ molecules from the active center. The contribution of this stabilization effect will be even more prominent if the concentration of these two molecules in solution is low. Structural reorganization of the enzyme active center, and the difference in energy for the binding of $preQ_1$ and $NADP^+$ may also affect the stability of the product, which were not accounted for in our model. A similar trend was also observed for stage 1. In this stage, the unstable product may be stabilized when the NADPH is included in the active center.

3.3. Roles of the catalytic residues

Our computational results and the available experimental data allow us to obtain a clear picture of the roles of the residues in the active site during the course of catalysis. The most prominent residue in this regard is Cys194. Early experimental results on the *B. subtilis* QueF[20] showed that the presence of the $preQ_0$ protected Cys194 (Cys55 in *B. subtilis*) from reacting with iodoacetamide, indicating that a covalent intermediate is presumably formed between $preQ_0$ and Cys194. More recently, crystal structures showed unambiguously the existence of such a thioimidate intermediate.[17] Sited-directed mutagenesis studies also confirmed that the enzyme loses its activity without this cysteine residue. The essential role of Cys194 for catalysis has become evident from our mechanistic study. Cys194 is covalently linked to the substrate in the first stage of the reaction, and the C-S bond formation is essential for the transfer of the first

hydride ion in stage two. Our calculations show that the intermediate (thioimidate) prior to the first reduction should be positively charged as the result of protonation and have a double bond character before the first hydride transfer. In the first hydride transfer, this configuration is possible only after the covalent-bond formation with Cys194. However, as discussed above, the C–S bond is inhibitory to the occurrence of the second hydride transfer; therefore, it must be broken in the third stage of the reaction.

Asp201 was also shown to be essential for the enzyme activity by mutagenesis studies.[13] Our calculations suggest that Asp201 is likely to be involved in all four stages of the nitrile reductase reaction. In the first stage, Asp201 accepts a proton from the thiol group of Cys194 and later donates the proton to the nitrile nitrogen atom of the substrate. In the second stage, Asp201 plays an indirect role in stabilizing the positively charged intermediate through very strong hydrogen bonding that allows Asp201 to delocalize some of the negative charge resulted from hydride transfer. In the third stage, Asp201 protonates the negatively charged sulfur atom of Cys194, which arises from the cleavage of the covalent C–S bond. Finally, in the fourth stage, Asp201 stabilizes the positively charged transition state and intermediate.

Because of its proximity to the nitrile group, one may assume that His233 acts as a general-base/acid catalyst during the catalysis. However, its role in the catalysis seems to be non-essential. His233 interacts either with Asp201 or with the substrate, but only via nonbonding interactions without any proton transfer. Glu234 is another residue that mutagenesis results have indicated as important for the catalytic mechanism.[13] Together with the X-ray crystallographic data,[15–17] we concluded that the major role of Glu234 is to bind and orient the $preQ_0$ substrate, rather than functional as a general-base/acid catalyst. And lastly, we found Thr197 to be important in the first stage of the reaction, because it stabilizes the negatively charged sulfur atom before the nucleophilic attack on the substrate.

4. Conclusions

We investigated the catalytic mechanism of *V. cholerae* QueF nitrile reductase by using the method of QM/MM calculation. The computational results suggest that the NADPH-dependent nitrile reduction is likely to proceed through four reactions stages. We obtained the kinetic barriers for the individual steps and elucidated the crucial conformational changes required for bond-breaking and forming events. The results together yield fresh insight into the catalytic mechanism of the highly unique process of biological nitrile reduction.

In the first stage of nitrile reduction, *i.e.* the formation of the thioimidate intermediate, the sulfur atom of Cys194 forms a covalent bond with the nitrile carbon of the substrate. This C–S bond formation occurs in two steps: (1) proton transfer from the thiol of Cys194 to Asp201, and (2) nucleophilic attack of the thiolate of Cys194 on the nitrile group of the substrate. The first proton transfer takes place rapidly and is reversible, with a low free energy barrier of 0.4 kcal/mol and a reaction energy of -3.5 kcal/mol. Upon some conformational changes of both substrate and the active-site residues, the nucleophilic attack occurs with a free energy barrier of 19.0 kcal/mol and a large positive reaction energy (13.7 kcal/mol). The unstable thioimidate intermediate is likely stabilized by the binding of NADPH. In the second stage, the thioimidate intermediate is reduced by NADPH to generate a thiohemiaminal intermediate. The hydride transfer form NADPH is relatively slow with a kinetic barrier of 19.1 kcal/mol and highly exothermic with a reaction energy of -14.9 kcal/mol. Again, Cys194 and Asp201 are the only amino acids that are directly involved in the reaction. The cleavage of the C–S bond occurs in the third stage. The first step of this stage is the cleavage of the C–S bond in the thiohemiaminal intermediate, which is a facile process with a barrier of 4.9 kcal/mol and a reaction energy of -2.3 kcal/mol. The second step is the protonation of the Cys194 sulfur by Asp201 with a very low kinetic barrier, although the reaction energy is very large (-24.3 kcal/mol) in magnitude, as a result of a conformational reorganization in the active site. Finally, hydride transfer from the second NADPH molecule to the imine intermediate occurs. This stage requires no direct involvement of active-site residues and is the rate-limiting step of the reaction, with a free

energy barrier of 20.8 kcal/mol. This result is in accordance with the turnover rate of the QueF homologs from various organisms, though there is no data for *V. cholerae* QueF. The reaction free energy for this step is positive (10.9 kcal/mol), which should be compensated by the entropic gain brought about as a result of the release of the $NADP^+$ molecule and the substrate. Overall, the mechanism we presented here is consistent with X-ray structural observations, kinetic data and site-directed mutagenesis results. We hope that the detailed catalytic mechanism will assist the current efforts of enzyme engineering and inhibitor design.

Acknowledgements

This work is supported by the GSK-EDB Green Manufacturing award to L.Z-X. H.H. thanks a Nanyang Assistant Professorship and the computational resources at the High-Performance Computing Centre at Nanyang Technological University. This work has been funded by Fundação para a Ciência e Tecnologia (FCT) through grant EXCL/QEQ-COM/0394/2012 (M.J.R. and P.A.F.). A.J.M.R. thanks FCT for a post-doctoral scholarship (SFRH/BPD/94883/2013)

References

(1) Iwata-Reuyl, D. *Bioorganic Chem.* **2003**, *31*, 24–43.

(2) El Yacoubi, B.; Bailly, M.; de Crécy-Lagard, V. *Annu. Rev. Genet.* **2012**, *46*, 69–95.

(3) Iwata-Reuyl, D. *Curr. Opin. Chem. Biol.* **2008**, *12*, 126–133.

(4) Durand, J. M. B.; Dagberg, B.; Uhlin, B. E.; Björk, G. R. *Mol. Microbiol.* **2000**, *35*, 924–935.

(5) Prasad, S.; Bhalla, T. C. *Biotechnol. Adv.* **2010**, *28*, 725–741.

(6) Kobayashi, M.; Nagasawa, T.; Yamada, H. *Trends Biotechnol.* **1992**, *10*, 402–408.

(7) Kobayashi, M.; Shimizu, S. *Nat. Biotechnol.* **1998**, *16*, 733–736.

(8) Yeom, S.-J.; Kim, H.-J.; Oh, D.-K. *Enzyme Microb. Technol.* **2007**, *41*, 842–848.

(9) Martínková, L.; Vejvoda, V.; Kaplan, O.; Kubáč, D.; Malandra, A.; Cantarella, M.; Bezouška, K.; Křen, V. *Biotechnol. Adv.* **2009**, *27*, 661–670.

(10) Yang, L.; Koh, S. L.; Sutton, P. W.; Liang, Z.-X. *Catal. Sci. Technol.* **2014**.

(11) Domínguez de María, P. *ChemCatChem* **2011**, *3*, 1683–1685.

(12) Wilding, B.; Winkler, M.; Petschacher, B.; Kratzer, R.; Glieder, A.; Klempier, N. *Adv. Synth. Catal.* **2012**, *354*, 2191–2198.

(13) Wilding, B.; Winkler, M.; Petschacher, B.; Kratzer, R.; Egger, S.; Steinkellner, G.; Lyskowski, A.; Nidetzky, B.; Gruber, K.; Klempier, N. *Chem. – Eur. J.* **2013**, *19*, 7007–7012.

(14) Moeller, K.; Nguyen, G.-S.; Hollmann, F.; Hanefeld, U. *Enzyme Microb. Technol.* **2013**, *52*, 129–133.

(15) Swairjo, M. A.; Reddy, R. R.; Lee, B.; Van Lanen, S. G.; Brown, S.; de Crécy-Lagard, V.; Iwata-Reuyl, D.; Schimmel, P. *Acta Crystallograph. Sect. F Struct. Biol. Cryst. Commun.* **2005**, *61*, 945–948.

(16) Kim, Y.; Zhou, M.; Moy, S.; Morales, J.; Cunningham, M. A.; Joachimiak, A. *J. Mol. Biol.* **2010**, *404*, 127–137.

(17) Chikwana, V. M.; Stec, B.; Lee, B. W. K.; Crécy-Lagard, V. de; Iwata-Reuyl, D.; Swairjo, M. A. *J. Biol. Chem.* **2012**, *287*, 30560–30570.

(18) Kim, Y.; Zhang, R.; Gu, M.; Anderson, W. F.; Joachimiak, A.; CSGID. *Be Publ.* **2011**, null – null.

(19) Reader, J. S.; Metzgar, D.; Schimmel, P.; Crécy-Lagard, V. de. *J. Biol. Chem.* **2004**, *279*, 6280–6285.

(20) Lee, B. W. K.; Van Lanen, S. G.; Iwata-Reuyl, D. *Biochemistry (Mosc.)* **2007**, *46*, 12844–12854.

(21) Lanen, S. G. V.; Reader, J. S.; Swairjo, M. A.; Crécy-Lagard, V. de; Lee, B.; Iwata-Reuyl, D. *Proc. Natl. Acad. Sci. U. S. A.* **2005**, *102*, 4264–4269.

(22) Vreven, T.; Byun, K. S.; Komaromi, I.; Dapprich, S.; Montgomery, J. A.; Morokuma, K.; Frisch, M. J. *J. Chem. Theory Comput.* **2006**, *2*, 815–826.

(23) Chung, L. W.; Hirao, H.; Li, X.; Morokuma, K. *Wiley Interdiscip. Rev.-Comput. Mol. Sci.* **2012**, *2*, 327–350.

(24) Berman, H. M.; Westbrook, J.; Feng, Z.; Gilliland, G.; Bhat, T. N.; Weissig, H.; Shindyalov, I. N.; Bourne, P. E. *Nucleic Acids Res.* **2000**, *28*, 235–242.

(25) Dennington, R.; Keith, T.; Millam, J. *Semichem Inc Shawnee Mission KS* **2009**.

(26) Maseras, F.; Morokuma, K. *J. Comput. Chem.* **1995**, *16*, 1170–1179.

(27) Svensson, M.; Humbel, S.; Froese, R. D. J.; Matsubara, T.; Sieber, S.; Morokuma, K. *J. Phys. Chem.* **1996**, *100*, 19357–19363.

(28) Dapprich, S.; Komaromi, I.; Byun, K. S.; Morokuma, K.; Frisch, M. J. *J. Mol. Struct.-Theochem* **1999**, *461*, 1–21.

(29) Becke, A. D. *J. Chem. Phys.* **1993**, *98*, 5648–5652.

(30) Lee, C.; Yang, W.; Parr, R. G. *Phys. Rev. B* **1988**, *37*, 785–789.

(31) Ditchfield, R.; Hehre, W. J.; Pople, J. A. *J. Chem. Phys.* **2003**, *54*, 724–728.

(32) Cornell, W. D.; Cieplak, P.; Bayly, C. I.; Gould, I. R.; Merz, K. M.; Ferguson, D. M.; Spellmeyer, D. C.; Fox, T.; Caldwell, J. W.; Kollman, P. A. *J. Am. Chem. Soc.* **1995**, *117*, 5179–5197.

(33) Frisch, M.; Trucks, G.; Schlegel, H.; Scuseria, G.; Robb, M.; Cheeseman, J.; Scalmani, G.; Barone, V.; Mennucci, B.; Petersson, G.; Nakatsuji, H.; Caricato, M.; Li, X.; Hratchian, H.; Izmaylov, A.; Bloino, J.; Zheng, G.; Sonnenberg, J.;

Hada, M.; Ehara, M.; Toyota, K.; Fukuda, R.; Hasegawa, J.; Ishida, M.; Nakajima, T.; Honda, Y.; Kitao, O.; Nakai, H.; Vreven, T.; Jr; Peralta, J.; Ogliaro, F.; Bearpark, M.; Heyd, J.; Brothers, E.; Kudin, K.; Staroverov, V.; Kobayashi, R.; Normand, J.; Raghavachari, K.; Rendell, A.; Burant, J.; Iyengar, S.; Tomasi, J.; Cossi, M.; Rega, N.; Millam, J.; Klene, M.; Knox, J.; Cross, J.; Bakken, V.; Adamo, C.; Jaramillo, J.; Gomperts, R.; Stratmann, R.; Yazyev, O.; Austin, A.; Cammi, R.; Pomelli, C.; Ochterski, J.; Martin, R.; Morokuma, K.; Zakrzewski, V.; Voth, G.; Salvador, P.; Dannenberg, J.; Dapprich, S.; Daniels, A.; Farkas; Foresman, J.; Ortiz, J.; Cioslowski, J.; Fox, D. *Gaussian 09 Revision D.01*; Gaussian Inc. Wallingford CT 2009, 2009.

(34) Ryde, U. *Proteins Struct. Funct. Bioinforma.* **1995**, *21*, 40–56.

(35) Ryde, U. *Protein Sci. Publ. Protein Soc.* **1995**, *4*, 1124–1132.

(36) Holmberg, N.; Ryde, U.; Bülow, L. *Protein Eng.* **1999**, *12*, 851–856.

(37) Wang, J.; Wang, W.; Kollman, P. A.; Case, D. A. *J. Mol. Graph. Model.* **2006**, *25*, 247–260.

(38) Case, D. A.; Darden, T. A.; Cheatham, T. E.; Simmerling, C. L.; Wang, J.; Duke, R. E.; Luo, R.; Crowley, M.; Walker, R. C.; Zhang, W. *Amber 10*; University of California, 2008.

(39) Wang, J. M.; Wolf, R. M.; Caldwell, J. W.; Kollman, P. A.; Case, D. A. *J. Comput. Chem.* **2004**, *25*, 1157–1174.

(40) Roothaan, C. C. J. *Rev. Mod. Phys.* **1951**, *23*, 69.

(41) Bayly, C.; Cieplak, P.; Cornell, W.; Kollman, P. *J. Phys. Chem.* **1993**, *97*, 10269–10280.

(42) McLean, A. D.; Chandler, G. S. *J. Chem. Phys.* **1980**, *72*, 5639–5648.

(43) Clark, T.; Chandrasekhar, J.; Spitznagel, G. W.; Schleyer, P. V. R. *J. Comput. Chem.* **1983**, *4*, 294–301.

(44) Frisch, M. J.; Pople, J. A.; Binkley, J. S. *J. Chem. Phys.* **1984**, *80*, 3265–3269.

(45) Marenich, A. V.; Jerome, S. V.; Cramer, C. J.; Truhlar, D. G. *J. Chem. Theory Comput.* **2012**, *8*, 527–541.

(46) Schrödinger, L. The PyMOL Molecular Graphics System, Version 1.6.0.0, 2010.

(47) Humphrey, W.; Dalke, A.; Schulten, K. *J. Mol. Graph.* **1996**, *14*, 33–38.

TOC Figure